We are IntechOpen, the world's leading publisher of Open Access books Built by scientists, for scientists

4,800
Open access books available

122,000
International authors and editors

135M
Downloads

Our authors are among the

154
Countries delivered to

TOP 1%
most cited scientists

12.2%
Contributors from top 500 universities

CLARIVATE ANALYTICS BOOK CITATION INDEX INDEXED

WEB OF SCIENCE™

Selection of our books indexed in the Book Citation Index in Web of Science™ Core Collection (BKCI)

Interested in publishing with us?
Contact book.department@intechopen.com

Numbers displayed above are based on latest data collected.
For more information visit www.intechopen.com

8

Time Resolved Spectroscopy with Femtosecond X-Ray Pulses

Enikoe Seres[1,2] and Christian Spielmann[1,2]
[1]*Institute of Optics and Quantumelectronics, Friedrich Schiller University Jena*
[2]*Helmholtz Institute Jena*
Germany

1. Introduction

Spectroscopy is of great interest for exploring the structure or composition of unknown matter. In 1813 Joseph von Fraunhofer discovered, independently from William Hyde Wollaston (1802), the dark lines in the spectrum of the sun, which has been later explained by the absorption of hydrogen. In 1859 Gustav Robert Kirchoff and Robert Wilhelm Bunsen discovered that the flame of gas burner changes its color, if different elements are heated up. In 1895 Wilhelm Conrad Röntgen (Röntgen, 1895) detected a new kind of radiation and named it X-ray radiation. In the first hundred years since their discovery, x-rays have played an important role in helping us understanding the structures of materials. Due to their short wavelength, x-rays are capable to resolve the structure of condensed matter but also the internal structure of atoms. The x-ray spectroscopic methods have been refined over the years. Nowadays physicists, chemists, biologists and material scientists rely on x-ray static structural analysis on a routine basis (Michette and Pfautsch, 1996).
In addition to the static structural information, transient structural information is required for a deeper understanding. Such dynamic processes include the breaking and formation of chemical bonds, protein motions, charge transfer, phase transitions and so on (Sundaram 2002; La-O-Vorakiat, 2009; Woerner 2010). In Figure 1, we summarize the main applications of the time resolved spectroscopy. Many of these problems have already been tackled by means of conventional optical pump/probe spectroscopy. Unfortunately, such optical measurements cannot be directly inverted to give the position of the atoms as a function of the times expect in very favorable cases. Unlike optical spectroscopy, x-ray diffraction (XRD) and x-ray absorption (XRA) do in principle provide direct ways to reconstruct the motion of atoms during dynamic processes. Thus, time-resolved XRD and XRA may serve as a more direct way to observe the microscopic processes by which biomolecules perform their tasks or to observe ultrafast processes in solid-state materials. An ideal x-ray system for time-resolved diffraction should have sufficient temporal and spatial resolution to resolve the dynamics of fast processes. It took almost one century since the discovery of x-rays to realize x-ray sources providing a temporal resolution which is sufficient to follow the atomic and molecular motion, or to monitor the dynamics of molecules such as rotation, vibration, dissociation, or to study the dynamics of electrons on their natural time scale. Atom motion takes place on a picosecond to femtosecond time scale, whereas attosecond resolution is

necessary for revealing the electron dynamics (Bressler et al., 2004, Rousse et al., 2001). Now, in the 21th century, we are in the fortunate situation to routinely generate bright femtosecond and attosecond x-ray pulses. In this chapter we review the current progress of time resolved x-ray spectroscopy and present some of our recent results about x-ray source development and x-ray absorption studies of transient states of matter. This chapter is divided into the following sections:

1. Introduction
2. X-rays and x-ray absorption spectroscopy
3. Pulsed x-ray sources
4. High harmonic generation
5. Time-resolved X-ray spectroscopy

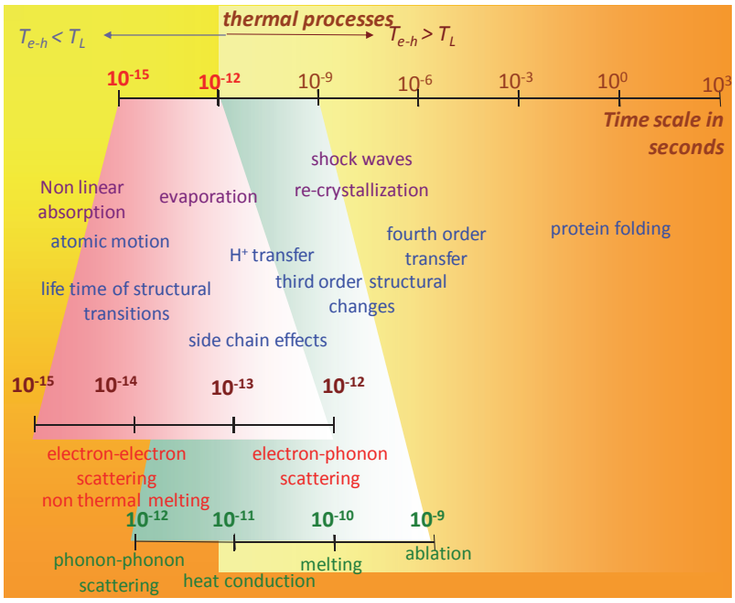

Fig. 1. Typical time scales for structural and electronic processes in solids.

2. X-ray radiation

X -ray radiation is a part of the electromagnetic radiation spectrum. The wavelength of X-rays, extends from 0.02 Å to 100 Å, and corresponds to the atomic and molecular length scales. X-ray radiation can be divided as follows:

- ultra-soft <1 keV (λ > 1 nm) and XUV
- soft 1 keV < E <10 keV as (0.1 nm - 1 nm),
- hard 10 keV < E < 100 keV (0.1 nm - 0.01 nm)
- ultra-hard E > 100 keV (λ < 0.01 nm)

The use of radiation in this wavelength range provides, direct information about the structure of matter (Agarwal 1991; Rose-Petruck et al., 1999; Bressler et al., 2002). Therefore, the development and application of X-ray sources for the structure determination is of great scientific interest. The first X-ray tube was realized by W. C. Röntgen. He discovered a new type of radiation arisen from the interaction of accelerated electrons with matter. The decelerated electron beam radiates a broad continuous spectrum with sharp characteristic

lines on it. The continuous part is referred to as "bremsstrahlung" and its maximum frequency depends only on the applied voltage and is independent of the anode material. The frequency of the line radiation depends on the anode material. The impacting electrons excite electrons from core levels into the continuum. The created hole is filled by an electron from a higher shell and the excess energy is emitted as a photon with an energy corresponding to the energy difference of the two involved states. For an anode material with atomic number Z, Moseley law predicts the frequency of the line:

$$\nu = R_{\infty} c \left(\frac{M}{m+M} \right) Z^2 \left(\frac{1}{n_f^2} - \frac{1}{n_i^2} \right) \quad (1)$$

Here m and M is the mass of the electron and the mass of the nucleus, n_f and n_i indicate the principal quantum number of initial and final states, R_∞ is the Rydberg constant.

2.1 X-ray spectroscopy methods

Both the bremsstrahlung and the characteristic radiation are used to investigate the structure of matter. Moreover, information about the atomic structure can be also obtained from the x-ray generation itself. The sample under investigation is illuminated with an electron or x-ray beam and its properties can be obtained by measuring the absorbed, diffracted, or scattered x-rays, the emitted x-ray fluorescence, or the ejected photoelectrons.

In the X-ray diffractometry (XRD) the X-ray beam interacts with the electron shells of the atoms fixed in a lattice. The diffraction pattern provides information about the atomic distances of the crystalline structure. At not too high photon energies, this scattering is elastic: there is no energy loss and then we also speak of coherent scattering (Rayleigh scattering). In this case, the wavelength of the scattered X-rays is the same as the original X-ray wavelength. When a core electron is ejected, then it may be followed by a recombination from higher occupied levels and a photon is generated. This effect is described and characterized by X-ray fluorescence (XRF). XRF is primarily only an element-specific method and allows not only qualitative but also quantitative analysis of the components contained in the sample volume. For special cases it can provide also information about the structure. X-ray spectroscopy for chemical analysis (ESCA) is based on the generation of photoelectrons. This technique is essentially limited to the surfaces. Typically, it is possibly to receive information from only two or three atomic layers, although the exciting X-rays penetrate much deeper.

X-ray absorption spectroscopy (XAS) provides information about the atomic structure and also about the atomic distances and chemical bonds. Matter can be characterized by the transmitted X-ray intensity I, if the sample is illuminated by an X-ray beam with intensity of I0:

$$I = I_0 e^{-\mu d}, \quad (2)$$

where d is the thickness of the material and μ is the linear attenuation coefficient. The incoming X-ray beam can excite core electrons to a higher unoccupied states or to the continuum. When the energy of the photons is increased, pronounced edges appears in the absorption spectrum, if the photon energy is high enough to excite electrons from a deeper core state (Figure 2) into the continuum.

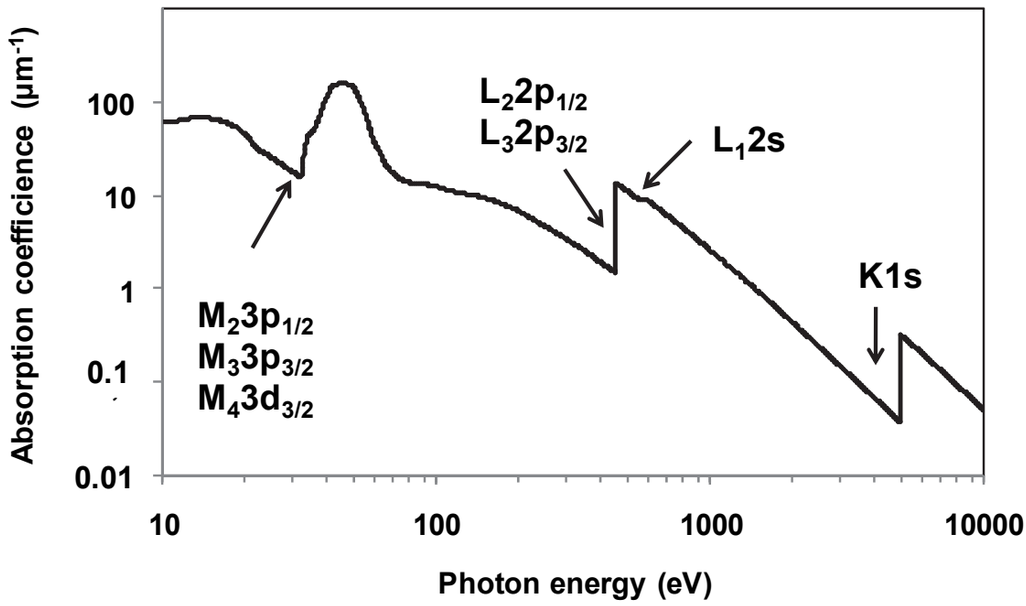

Fig. 2. X-ray absorption spectrum of Ti with K, L and M-edges.

A closer examination shows that only the K-edge consists of a simple jump. Near the L-absorption edge well-resolved jumps can be seen. The M-edges are not so well resolved.

2.1.1 Fine structure of the XAS signal

If the X-ray absorption spectrum is measured with high resolution, then a fine structure can be observed and resolved. The position and shape of the absorption edges is determined by the atom and is independent from environment of the atom, at least in a first approximation. The reason is that the x-ray absorption is related to the core levels, and only electrons from outer shell are involved in chemical bonds. However spectroscopy with sufficiently high resolution can detect an influence of the chemical bond on the energy and structure of the absorption edges. For determining the structure, i.e. getting information about the neighborhood of the atom of interest, we can rely on the following X-ray absorption methods:

- XAMES (X-Ray Absorption Main Edge Spectroscopy). The position of the absorption edge contains information about the electronic structure of atoms and the structure of the material. The pre-edge contains further information about the electron configurations and the symmetry around the absorbing atom. The measurements are made in a range from -10 eV to +10 eV around the absorption edge of the atom. The shift of the edge position is often referred as "chemical shift".
- XANES (X-Ray Absorption Near Edge Spectroscopy) provides information on the valence electrons and chemical bonds. It is necessary to record the signal in a range of 10 – 40 eV above the edge.
- EXAFS (Extended X-Ray Absorption Fine Structure) contains structural information, i.e. the distance to the neighboring atoms. The absorption spectrum is measured and evaluated in a range from 40 eV to 1000 eV beyond the absorption edge.

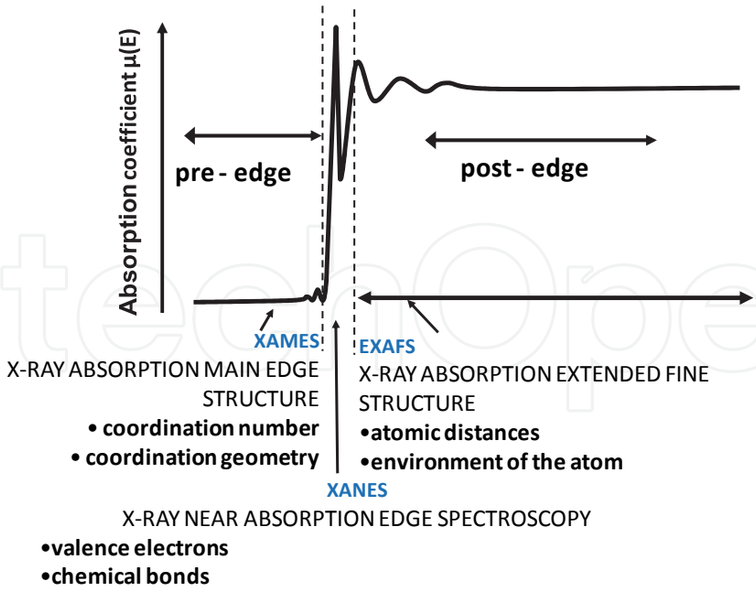

Fig. 3. Structure of the absorption edge can be divided into the ranges of XAMES, XANES and EXAFS.

2.1.2 EXAFS signal at the K-edge

In principle, structural information can be obtained with XANES or EXAFS. The measurement in a narrow range is easier, but XANES does not allow a simple determination of the distance to the next atoms from the experimental data. The basic principle of EXAFS is summarized in the following. The incident photons excite an electron from a core level into the continuum. The generated and outgoing photoelectron waves are elastically scattered by neighboring atoms. Quantum mechanically speaking, part of the wave function of the photoelectron is reflected by the neighboring atoms and the wave functions interfere. The modulation in the absorption spectrum depends on the path difference of the partial waves, and at a fixed atomic distance it is a function of the incident X-ray photon energy. (Stern 1974; Lytle et al., 1975; Lee et al, 1981; Rehr et al, 1992; Rehr & Albers 2000; Sipre, 2002.) The evaluation of a measured EXAFS spectrum requires the following steps. First, $\chi(E)$, the normalized EXAFS signal is calculated from the measured absorption spectrum:

$$\chi(E) = \frac{\mu(E) - \mu_0(E_0)}{\Delta\mu_0(E_0)}, \tag{3}$$

where $\mu(E)$ is the measured absorption coefficient, $\mu_0(E)$ is the smooth background function, or the absorption coefficient of the atom, and $\Delta\mu_0(E_0)$ is the measured jump of the absorption $\mu(E)$ at the edge and the energy of the absorption edge is E_0. Then the signal is converted into k-space: $k = \sqrt{\frac{2m_e}{\hbar^2}(h\nu - E_0)}$, where hv is the incident energy of X-ray photons. The calculated signal $\chi(k)$ carries information about the distances and the type of neighboring atoms:

$$\chi(k) = \frac{1}{k}\sum_j \frac{N_j \left| f_j(k,\pi) \right|}{kr_j^2} \sin\left[2kr_j + \Psi_j(k)\right] \cdot e^{-2k^2\sigma_j^2} e^{-\frac{2r_j}{\lambda_j(k)}}$$

amplitude

wave number of the photo electrons $k = \sqrt{\frac{2m_e}{\hbar^2}(h\cdot\upsilon - E_0)}$

phase

Debye-Waller-factor

correction term

Here, N_j is the number of backscattering atoms at the same distance r_j from the absorber atom. f(k) and Ψ(k) corresponds to the amplitude and phase shift of the scattered wave, and σ^2 is the standard deviation of atomic distance. The factor $e^{-2k_j\sigma_j^2}$ also known as Debye-Waller factor is a measure for the smearing of the interference signal. Due to the spatial dispersion of the outgoing wave only backscattering from the next neighbors must be considered. Furthermore, the photoelectron must be scattered before the generated hole was filled. If these approximations are not valid a correction term of $e^{2r_j/\lambda_j(k)}$ is required. The size $\lambda_j(k)$ depicts the energy-dependent mean free path of photoelectrons. Phase shift impressed on the scattered electron wave is given

$$\Psi_j(k) = \Phi_j(k) + 2\delta_l(k) \tag{4}$$

with $\Phi_j(k)$ phase shift through the backscattering from the j^{th} neighboring atom and δ_l is the phase shift of the photoelectron in the potential of an atom in the l^{th} shell. The amplitude of the backscattered wave is given:

$$f(k,\pi) = \left| f(k,\pi) \right| e^{i\Phi(k)} = \frac{1}{2ik}\sum_l (2l+1)\left(e^{2i\delta_l} - 1\right)(-1)^l \tag{5}$$

With the help of the given formalism, the atomic distance can be precisely determined by EXAFS. Additionally it may be necessary to determine the composition of the nearest neighbors by other methods (Bzowski et al., 1993; Filiponi et al., 1989; Johnson et al.; 2003, D'Angelo et al., 1996, Bianconi et al., 1987, Farges et al., 1997; Faraci et al., 1997).

2.1.3 EXAFS signal at the L-edge

Previously it was assumed that the electron is generated by an excitation from the K-shell. However, EXAFS is also possible from e.g. the L-shell. For considering absorption from the L_1 shell, the same formalism as for the K-shall can be used. However for electrons from the $L_{2,3}$ shell the evaluation is more complicated. The reason is that the electron in the initial state is a p-state instead of a s-state. Because of the selection rule, the photoelectron generated can be a s or d-like electron. The difference is not only the energy but also the phase in the scattering is different and in addition, there is a superposition of two states. For EXAFS from the $L_{2,3}$ shell the signal can be calculated according to the following formula:

$$\chi(k)=\frac{1}{k}\sum_j \left\{ \begin{array}{c} \frac{1}{2}\left(1+3\cos^2\Theta_j\right)M_{21}^2\sin\left[2kr_j+2\delta_2(k)+\Phi_j(k)\right]+ \\ +\frac{1}{2}M_{01}^2\sin\left[2kr_j+2\delta_0(k)+\Phi_j(k)\right]+ \\ +M_{01}M_{21}\left(1-3\cos^2\Theta_j\right)\sin\left[2kr_j+\delta_0(k)+\delta_2(k)+\Phi_j(k)\right] \end{array} \right\} \cdot \tag{6}$$

$$\cdot\left(M_{21}^2+\frac{1}{2}M_{01}^2\right)N_j\frac{\left|f_j(k,\pi)\right|e^{-2k^2\sigma_j^2}}{kr_j^2}e^{-\frac{2r_j}{\lambda_j(k)}}$$

where M_{01} and M_{02} are the elements of the radial dipole matrix between the l = 1 initial state and the l = 0 and l = 2 final state. The measured signal depends also on the orientation of the atoms. In the case of polycrystalline material, the third term of equation (6) disappears. Additionally the transition probabilities have been calculated and the p to d transition dominates over the p to s transition by a factor of 50, so the second term can be neglected. In a first approximation EXAFS spectra from the L-edge can be evaluated with the same simple approach as spectra above the K-edge.

3. X-ray sources

Synchrotrons represent the major source of powerful X-rays and will continue to play a dominant role for X-ray science in the foreseeable future. Nevertheless, a wide range of X-ray applications in science, technology and medicine would greatly benefit from i) X-ray pulse durations much shorter than routinely available from synchrotrons (few hundred picoseconds), ii) synchronizability of ultrashort pulses to other events, and iii) availability of useful fluxes from compact laboratory X-ray sources. Triggered by these needs, we witnessed in the last few years huge attempts towards the realization of such x-ray sources.

Advances in ultrashort-pulse high-power laser technology over the last decade (Perry and Mourou, 1994; Umstadter et al., 1998) triggered extensive research activity aiming at the development of compact, versatile laboratory X-ray sources in a number of laboratories for ultrafast as well as other applications. As a result, ultrashort-pulsed X-ray radiation became available from femtosecond-laser-produced plasmas (FLPP), (Murnane et al., 1991; Giulietti and Gizzi, 1998; and references therein).

These sources are now capable of converting up to several per cent of the driving laser pulse energy into incoherent X-rays emitted in a solid angle of 2π-4π and delivering pulses with durations down to the subpicosecond regime. FLPP sources matured to a point where a wide range of applications can be tackled all the way from the soft to the hard X-ray regime. Already demonstrated examples include time-resolved X-ray diffraction and absorption spectroscopy (Raksi et al., 1996; Rischel et al., 1997; Rose-Petruck et al., 1999) and medical radiology with improved contrast and resolution (Gordon III et al., 1995).

Many laboratory X-ray applications would greatly benefit from or rely on (spatially) coherent sources with high average and/or peak power. One of the major approaches to laboratory production of coherent X-rays is the development of X-ray lasers. Whereas short-wavelength lasing has been successfully demonstrated with compact, table-top setups using several promising schemes at λ > 15 nm in the XUV range (Rocca et al., 1994; Lemoff et al., 1995; Nickles et al., 1997; Korobkin et al., 1998), lasing at shorter (soft-X-ray) wavelengths

could only be achieved at large-scale facilities so far (Nagata et al., 1993; Da Silva et al., 1994; Zhang et al., 1997).

Another promising route to developing compact coherent X-ray sources is high-order harmonic generation (HHG) with ultrashort-pulse lasers (L'Huillier and Balcou, 1993; Macklin et al., 1993; Wahlström et al., 1993; Perry and Crane, 1993; Kondo et al., 1993). Extensive theoretical (Lewenstein et al., 1994; Antoine et al., 1996) and experimental (Salieres, 1995; Ditmire et al., 1995, 1996) research provided valuable insight into the microscopic (strongly-driven atomic dipole) and macroscopic (propagation effects, e.g. phase mismatch) phenomena relevant to HHG (for a review see Salieres et al., 1999). Recent investigations revealed that ultrashort drivers with pulse durations well below 100 fs (Zhou et al., 1996) can produce HH conversion efficiencies comparable to XUV lasers in the 50 – 20 nm range, $\eta_{conv} \approx 10^{-5} - 10^{-7}$, respectively (Sommerer et al., 1999; Constant et al., 1999).

Recently, few-cycle, sub-10 fs laser pulses produced HH radiation at 13-10 nm with efficiencies in the range of $\eta_{conv} \approx 10^{-7} - 10^{-8}$ and with pulse durations estimated as < 3 fs at a repetition rate of 1 kHz, resulting in the highest average and peak powers ever demonstrated from a coherent laboratory soft-X-ray ($E_{ph} \geq 100$ eV) source (Schnürer et al., 1999). Pulses in the 5-25 fs range have extended HHG even down to the water window, 2.3 - 4.4 nm (Spielmann et al., 1997; Schnürer et al., 1998). Theoretical investigations suggest that few-cycle-driven harmonic emission is confined temporally to a tiny fraction of the laser period in the cut-off region of the spectrum (Kan et al., 1997; Christov et al., 1997; Spielmann et al. 1998), resulting in a single XUV/X-ray burst of attosecond duration.

SOURCE	PHOTONS /PULSE/ 0.1% BW	PULSE WIDTH	ENERGY RANGE	REPETITION RATE
High Harmonic Generation		≥80 as	< 4 keV	kHz
Laser generated plasmas	10^2	~300 fs	≤ 3 keV	10 Hz- 1 kHz
Third generation synchrotrons	10^4-10^6	10-20 ps	0- 100 keV	≤ 500 MHz
Slicing scheme	10^1-10^3	~100 fs	0-100 keV	1-10 kHz
Short pulse photon source (SPPS)	10^8	~ 100 fs	Fixed energy	10 HZ

Table 1. Summary of the x-ray sources usable for time-resolved x-ray spectroscopy.

In spite of these advances, applications of coherent laboratory X-ray sources are at the beginning. E.g. the photon fluxes available from state-of-the-art harmonic sources are still low, and allow only selected experiments. However, increasing the power of the few-cycle-driven harmonic source by 1-2 orders of magnitude holds promise for opening up further intriguing application fields in science and technology and pushing the frontiers of physical sciences. The former include X-ray spectroscopy, X-ray microscopy, X-ray

photoelectron spectroscopy and possibly X-ray interferometry all of which have had to rely on large-scale synchrotron facilities far. The unprecedented pulse durations and X-ray peak intensities that may become available from harmonic sources, opening the way to attosecond science.

4. High harmonic generation

High harmonics (HH) are generated by the interaction of intense linearly polarized laser pulses with atoms, molecules or atomic clusters, where photons are generated in the extreme ultraviolet spectral region and in the soft X-ray regime. The generation takes place in a gas jet with a focused, ultrashort, intense laser pulse. The relatively modest demands on the parameters of the laser pulses and the excellent temporal and spatial coherence of high harmonics pave the way for developing a brilliant compact short-wave radiation source. The rapid progress in high harmonics generation has made it possible for the first time to realize sophisticated inner-shell spectroscopy with a compact laboratory system.

These achievements are mainly based on the rapid development of ultrashort pulse lasers. With them, it is possible to build small, stable and high repetition laser systems. The intensity also plays an important role, since the maximum photon energy is directly proportional to it. Despite a number of advantages and excellent properties of HH sources they have the weakness of the relatively low conversion efficiencies of visible or near-IR laser light into XUV radiation. HH generation is a coherent process, so the signal grows quadratically with the propagation length. The fortunate length scaling is only applicable, if the generated short wavelength radiation remains in phase with the generating laser, which is termed as phase matching. If the condition for phase-matching is not fulfilled, the signal grows only along the often very short coherence length. Beside the linear (atomic) dispersion the major contribution to the phase mismatch is the plasma dipersion of free electrons. During the interaction of the laser pulse width the atoms, not only XUV photons are generated, but also lots of free electrons. The shorter the wavelength, the higher must be the laser intensity and the higher is the free electron density and larger the phase mismatch. So a major task in HHG is the development of phase-matching or quasi-phase matching schemas to extend the coherence length and hence the obtained photon flux. In this section we will briefly review the theoretical description of HHG and will present experimental results on approaches to extend the phase matching length.

To describe the process qualitatively, a bound electron can be released in the presence of a strong laser field by tunneling ionization, which can be only treated by applying quantum-mechanic. The subsequent motion of the free electron will be described by the classical equations of motions. The free electron first is accelerated away from its parent ion, and after changing the polarity of the field, it is accelerated toward the ion again. The returning electron can recombine and the excess energy is emitted as a photon with an energy corresponding to the binding energy plus the kinetic energy at the instant of recombination. The highest photon energy, the so called cut-off in the harmonic spectrum corresponds to the maximum energy and can be written:

$$N_c \hbar\omega_0 = W_b + 3.17U_p \tag{7}$$

Where W_p is the ionization potential, N_c the number of the "cut-off" harmonics and $U_p = \frac{e^2 E_a^2}{4m\omega_0}$ is the ponderomotive potential, with the electron charge e and electron mass m, the frequency ω_0 and amplitude E_a of the laser field. This process is repeated in each optical cycle twice and the signal has a point symmetry compared to time zero. These two findings imply, that the spectrum will only contain the odd harmonics of the laser frequency. At very high intensities, the speed of the electron will be comparable to the speed of light. In this relativistic case, we must also consider the influence of the magnetic field on the motion of the electron. The resulting trajectories did not show a return to its parent ion, so no high harmonic signal will be generated.

However, for a more detailed description and explaining features like conversion efficiency and so on we must rely on a quantum mechanics. The nonlinear response of an atom to intense radiation can be divided into different intensity-dependent processes. At low and moderate intensity, if the external electric field is smaller than the static Coulomb field (perturbative nonlinear optics), the laser field modifies the atomic states: the energy levels are shifted by an energy proportional to electric field strength E_a which is known as Stark shift. The border between the region of the perturbative and nonpertubative nonlinear optics is determined by the following equations:

$$\frac{\chi^{(k+1)}E^{k+1}}{\chi^{(k)}E^{k}} \approx \frac{eE_a a_B}{\hbar\Delta} = \alpha_{bb} << 1 \ (Bound-bound\ \ Transition) \tag{8}$$

$$\frac{1}{\gamma} = \frac{eE_a}{\omega_0\sqrt{2mW_b}} = \frac{eE_a a_B}{\hbar\omega_0} = \alpha_{bf} << 1 \ (Bound-free\ Transition) \tag{9}$$

With e the elementary charge, m the mass of the electron, $W_b > \hbar\omega_0$ is the binding energy, $a_B = \frac{\hbar}{\sqrt{2mW_b}}$ the Bohr radius, E_a is the time-dependent amplitude of the linearly polarized radiation, and γ is a scaling parameter, the Keldysh parameter (Brabec et al., 2000). If the laser field is comparable to the binding Coulomb field ("Strong Field" area), the binding potential is deformed and a potential barrier appears. An initially bound electron can now tunnel through this barrier in a fraction of the laser - oscillation - cycle (T_0). Then, the electron follows adiabatically the variation of the optical field. It can move significantly away from its original position and acquires high kinetic energy (Brabec et al., 2000). The production of HH radiation takes place on the return of the electron to its parent ion.

The maximum energy E_c of the generated harmonic photons and the shape of the emitted spectrum critically depends on how and when the ionization takes place. The ionizing electric field is $E(t) = \tilde{E}_a(t)e^{-i\omega_0 t + i\phi_c} + c.c.$ where the electric field with amplitude E ($E_a = 2\left|\tilde{E}_a\right|$) and with a frequency of ω deforms the atomic binding potential. Through the formed barrier, the electron can tunnel with a frequency of $\omega_t = \frac{E}{\kappa} = \frac{2E}{E_0}\omega_0$, where $\gamma = \frac{\omega}{\omega_t} << 1$ (Ammosov 1986, Krainov 1997). The dipole apprioximation assumes a linearly polarized laser field, and requires the validity of the following assumptions:

- All bound states except the ground state are neglected.

- The laser intensity is lower than the saturation intensity, so the ground state is not depopulated.
- In the continuum the electron can be treated as free particles. The influence of the potential of the ion is negligible.

For very high intensities, however, the validity of the dipole approximation must be questioned and it is necessary to extend the theory with multi pole effect (Walser et al., 2000) to obtain an adequate description.

The emission of harmonic radiation from single atoms is determined by the $\frac{d^2}{dt^2}\langle\Psi|r|\Psi\rangle$ dipole acceleration arising as the solution of the Schrodinger equation. Here r is the vector of space and ψ is the wave function of the electron. Under the assumption of γ < 1, the quantum-mechanical expected value of the generation of high frequencies <D(t)> can be represented as a product of three atomic probability amplitudes:

$$\langle D(t)\rangle = \sum_{t_b} \frac{1}{\sqrt{i}} a_{ion}(t_b) a_{prop}(t_b, t) a_{rec}(t) \tag{10}$$

The electron can be released at the time t_b with the probability of $a_{ion}(t_b)$ by tunneling ionization. After that, it propagates in the laser field and returns back at time t with probability $a_{prop}(t_b, t)$ to the origin atom, where fall back to the ground state width the recombination probability of $a_{rec}(t)$ and creates a photon. The sum shows that there are several possible values for t_b. The resulting dipole emission spectrum is discrete and consists only of odd multiples of the fundamental laser frequency ω_0.

The conversion efficiency of high harmonic radiation is defined by the generation processes and the propagation processes. (Lewenstein et al., 1994; Scrinzi et al., 1999). Unfortunately, we do not have easily accessible experimental parameters to optimize the generation process, but there are several methods to enhance the signal by controlling the propagation. As for all coherent processes the signal grows only over the coherence length, i.e. as long as the condition for phase matching is fulfilled. In the following we discuss the major effects limiting the harmonic yield:

- Absorption of the radiation. During the propagation in the gas, the harmonic beam excites the core electrons and is re-absorbed. Although the absorption can be minimized by reducing the gas pressure or shortening the length of the gas jet, but it also reduces the conversion efficiency. It has been also shown that in the short wavelength range the absorption length is much longer than the coherence length and it is no longer the primary limitation. Its influence can be further reduced, by keeping the background pressure as low as possible in the vacuum system for generating and detecting HH radiation.
- Loss of phase matching. There are three effects that contribute to a phase mismatch. First, the phase shift between the HH pulse and the laser pulse by the dispersion of the free electrons background. Most of the freed electrons will not recombine, and remain as free electron background in the interaction region. The resulting coherence length is $L_{fe} = \frac{2\pi c\omega_0}{\omega_p^2(\tau)N}$, where $\omega_p = \sqrt{\frac{e^2 n_e}{m\varepsilon_0}}$ the plasma frequency, depending on the free-electron density n_e. Secondly, the curved wave front of the laser pulse (focused Gaussian beam)

produces a phase factor, which corresponds to a negative contribution to the refractive index. The corresponding coherence length is given by $L_{g,fs} = \frac{\pi z_0}{N} = \frac{\pi^2 w_0^2}{N\lambda_0}$, where z_0 and w_0 are the confocal parameter and the radius of the beam waist. This contribution is particularly large in the vicinity of the focus of the laser beam; therefore it is convenient to place the gas jet either before or after the focus, to minimize this contribution. Thirdly, the dispersion of the refractive index of the gas also causes dephasing. Since the refractive index is very close to 1 for the gas at the laser wavelength, and at the XUV wavelength it is approximately 1, this contribution is small and can be often neglected.

- Defocusing of the laser. During high harmonic generation, the laser pulse creates a free-electron density profile, which causes defocusing. This effect can be compensated with a spatially formed laser pulse profile. (Brabec et al., 2000).

After propagation over a distance longer than the coherence length, the generated x-rays destructively interfere with the already generated beam. Introducing a suitable long gap, where only propagation and phase shift happen, the signal can be enhanced in a subsequent region once again. Compared to the perfectly phase-matched case, quasi-phase-matching (QPM) leads to lower conversion efficiency, but for HH, QPM with its periodic structure is the only choice, because perfect phase-matching cannot be realized. Several implementations of this technique have been realized, including spatially modulated hollow fibers or using a gas jet sequence (Gibson et al., 2003, Paul et al., 2003, Zepf et al., 2007; Seres et al., 2007). Using a sequence of gas jet sequence, QPM has been successfully realized over a wide spectral range around 300 eV (Seres et al., 2007), see figure 4.

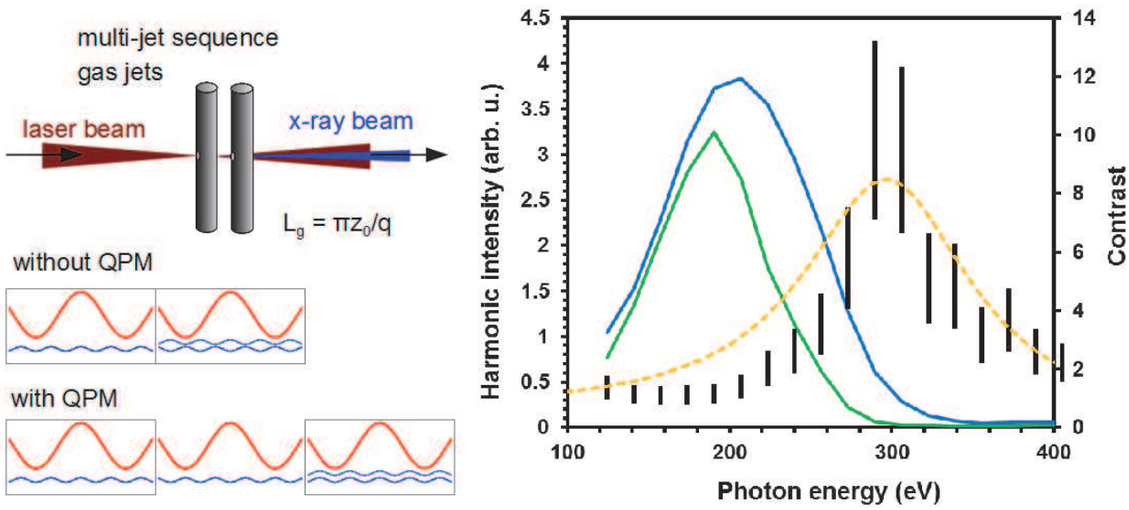

Fig. 4. Principe of the quasi-phase matching at 300 eV using two gas jets. When the two jets are merged (without QPM), the generated x-ray beams interfere destructively in the second jet and the photon yield after the second jet (green) is smaller than it would be after the first jet. When the two jets are moved to a suitable distance (with QPM), the generated x-rays in the second jet constructively interfere with the x-rays generated in the first jet. The photon yield (blue) get larger and the enhancement (black error bars) can be up to one order of magnitude with good agreement with the theory (orange dashed line).

Especially for radiation above 100 eV, the coherence length can be as short as a few microns representing a severe limitation for the obtainable flux. However, the conversion efficiency can be substantially increased by applying the method of nonadiabatic self-phase matching (NSPM) (Seres, 2005, 2006a). As mentioned above the free electron background strongly modifies the phase velocity for the laser beam. As a consequence the radiating atoms are no longer in phase, limiting the achievable flux. Recently it was shown, if the free electron density changes substantially within one optical cycle, the phase velocity of the laser beam will be strongly modified. Choosing the laser parameter right, i.e. the peak intensity should be one order of magnitude above the ionization threshold and the pulses should consist of only few cycles, this ionization induced phase shift cancels the free electron phase shift. This process is known as nonadiabatic self-phase matching (NSPM) (Tempea et al., 2000). With this method it was possible to extend the phase matching length by orders of magnitude even in the keV photon energy range and generate more than 2000th harmonics of Ti:sapphire laser wavelength of 800 nm (1.54 eV) with improved photon yield (Seres et al., 2004; Seres et al., 2005; Seres et al., 2006a). Figure 5 shows a typical spectrum generated in Ne gas with the 12-fs-long, 2.5-mJ pulses of a Ti:sapphire laser system (Seres et al., 2003).

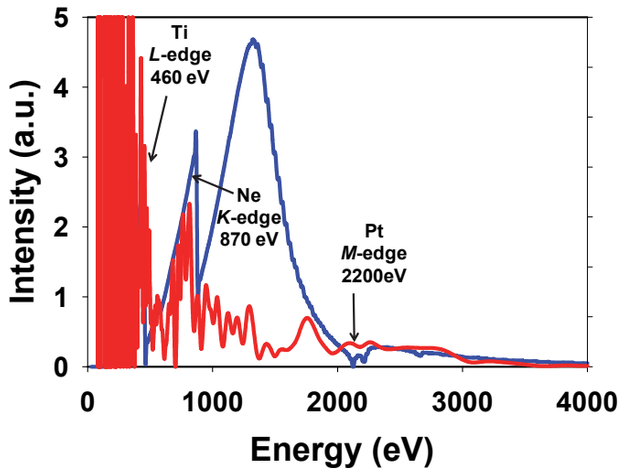

Fig. 5. Measured high harmonic spectrum (red) generated in Ne gas with the 12-fs-long, 2.5-mJ pulses of a Ti:sapphire laser system. The absorption edges of the used Ti foil, the used Ne gas and the Pt coating of the x-ray grating are well recognizable on both the measured spectrum and the calculated transmission curve (blue).

5. Time resolved x-ray spectroscopy

There is a broad spectrum of ultrafast processes in nature. For an experimental investigation we trigger the ultrafast process, i.e. we introduce an instantaneous structural change, with an ultrashort light pulse, the pump pulse. The characteristic of the material is probed by another light pulse with an adjustable delay in respect to the pump pulses. In an conventional pump-probe experiment both pulses are in the visible optical range. The development of reliable femtosecond solid-state laser brought new possibilities into time-resolved spectroscopy (Zewail 2000). For the first time it became possible, in principle to monitor the nuclear motion of molecules, crystal lattices and other out-of-equilibrium structures. However, usually it is very difficult to map the experimental observations to the

structural dynamics. Therefore, experimental approaches are needed which can overcome the limitation of optical studies for structural determination, while the high temporal resolution of femtosecond lasers is maintained. Techniques such as X-ray diffraction (XRD) (Rousse 2001), X-ray absorption spectroscopy (Nakano 1999), or X-ray photoelectron spectroscopy deliver much more direct information about the structure. The key to the successful realization is the development of laser driven x-ray sources. Various schemes have been demonstrated but all of them rely on availability of state of the art femtosecond solid-state laser system. In this section we will describe our apparatus, which allowed for the first time time-resolved x-ray absorption spexctroscopy with femtosecond resolution.

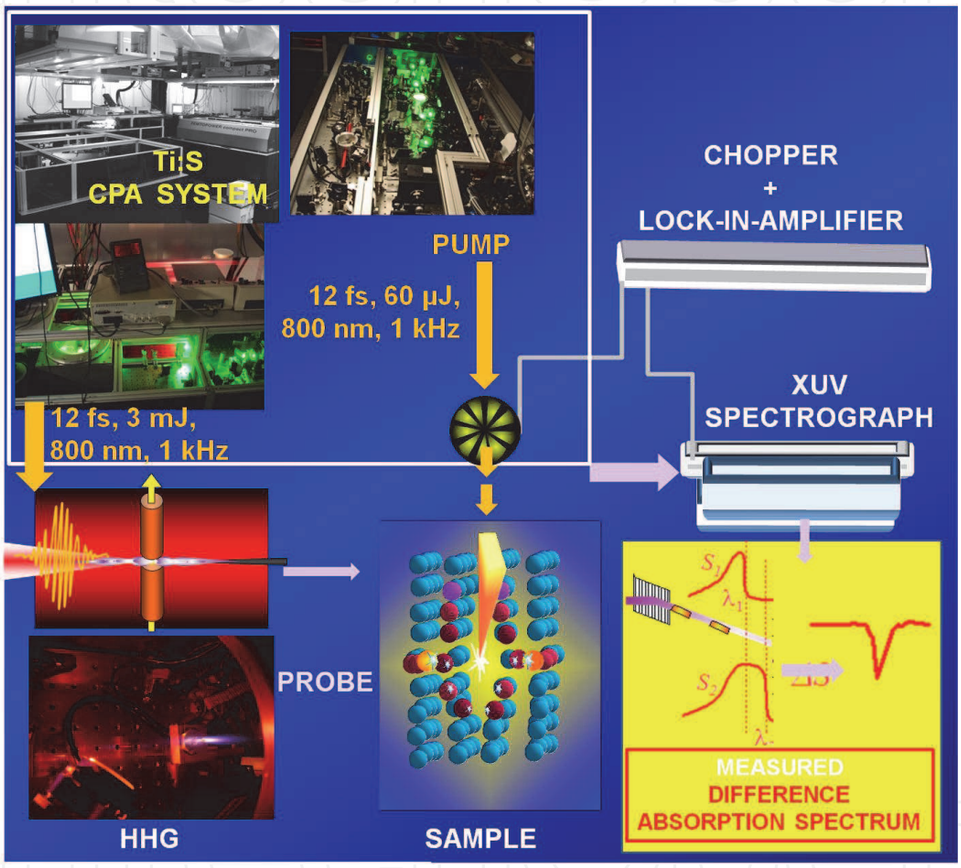

Fig. 6. Experimental setup for time-resolved x-ray absorption spectroscopy. A Ti:sapphire based CPA laser systems delivers energetic ultrahsort pulses. In a gas jet the laser pulses upconverted into the XUV range via high harmonic generation. The sample is pumped by a visible laser pulse. The structural changes are probed with a delayed XUV pulse. With a lock in amplifier and a spectrometer we can measure the XUV difference absorption spectrum, i.e. the change of the spectrum between the pumped and unpumped case.

Our pump-probe experimental setup is based on a state-of-the art multi pass Ti:sapphire CPA amplifier system. The front-end of the system is a mirror dispersion controlled Ti:sapphire oscillator delivering 10 fs, 5 nJ pulses. After a gentle stretching of the pulses to few picoseconds the pulses are amplified in a ten pass amplifier to amplifier to more than 1 mJ more than 1mJ at a repetition rate of 1 kHz. The pulses are compressed with double

prism compressor to less than 30 fs and a final energy of 800 μJ. Such short pulses after compression are only possible by carefully compensating the residual high order dispersion with chirped mirrors and specially designed filters to counterfeit gain narrowing. Further spectral broadening is obtained with a hollow fiber filled with Ne. The output spectrum has a width supporting pulses in the order of 10 fs.

The phase and amplitude of the broadened pulses are shaped with an acousto-optic-modulator ("DAZZLER"), which proved later to be an indispensable tool for high harmonic optimization. The broadened and shaped pulses are launched into a second and third amplifier stage and finally compressed with triple-prism-compressor (Seres et al., 2003). After the third amplifier stage the compressed pulsesare 12 to 15 fs long and the pulse energy is 3 mJ. Adding an additional compressor stage consisting either of a filament (Seres et al., 2007) or a gas filled hollow-core fiber (Seres 2006a) and chirped mirrors we were able to compress the pulses down to 5–6 fs with energy in the range of 1–2 mJ. These laser pulses were up-converted in a noble gas jet into XUV via high harmonic generation. For maximizing the photon yield we applied quasi phase matching (Seres 2007) and NSPM (Tempea 2000, Seres 2004)

For the quasi-phase matching experiments we need intense pulses as short as possible. The output pulses of this system were spectrally broadened in an Ar filament and compressed with chirped mirrors to about 6 fs at pulse energies of 1.5 mJ. With a spherical mirror the pulses were focused into a sequence of two gas filled nickel tubes with a diameter of 0.2 mm. With a backing pressure of 80 mbar in He, the highest HH yield in the 400–600 eV spectral range was reached with a jet distance of 1.3 mm (Seres 2007).

For non-adiabatic technique, the 3 mJ, 12 fs laser pulses were strongly focused into a Nickel tube filled with Ne or He reaching an intensity of 2×10^{16} W/cm². The laser beam interacted with He atoms in 0.4-mm-long volume. The fast ionization gave the proper addition to the phase matching terms, so we could reach approximately the 2000^{th} harmonics of the laser frequency corresponding to photon energies in the order of 3500 eV (Seres 2006a, 2006, Seres 2004). The broad spectrum of the x-ray pulses is well suited for static x-ray absorption spectroscopy. Different thin foils were inserted (200-nm-thick copper, 1-μm-thick aluminum, 300-nm-thick silicon) into the x-ray beam and the transmitted spectra were recorded with a scanning x-ray monochromator (248/310G, McPherson) equipped with a photoelectron multiplier Channeltron® 4715G. The absorption edges of Cu, Al, and Si at 0.94, 1.5, and 1.8 keV were clearly resolved, respectively. The shape of the measured spectra below and slightly above the absorption edge contains no information, which is of interest in our study.

5.1 Time resolved x-ray spectroscopy with HH radiation in material science

In this section we report on the generation of soft x-ray pulses via high harmonic generation and their first use for time resolved x-ray absorption spectroscopy (XAS) to investigate the structural dynamic of amorphous silicon with a temporal resolution of about 20 fs. To our knowledge this is the highest temporal resolution ever demonstrated in XAS (Seres E. 2008).

To tackle time-resolved XAS in the soft x-ray regime the light source must meet the following requirements: a) it must provide continuum radiation, b) it must provide ultrafast pulses, and c) it should have a sufficient photon flux (Bressler 2004). We realized it via high harmonic generation. HHG is a line radiation, and therefore of limited use for XAS. However, using very short driving laser pulses the line spectrum becomes continuous near the cut off (Brabec 2000). Due the generation process the XUV pulses are also always shorter

than the driving laser pulses. The short pulse duration and the excellent spatial and spectral characteristic make HHG based sources well suited for time-resolved XAS.
Our pump-probe experimental setup based on a single-stage Ti:sapphire CPA amplifier system. Most of the energy of the output beam was tightly focused with a broadband mirror with a focusing length of 150 mm into a Ne gas jet at an intensity of about 10^{15} W/cm^2. The XUV radiation hits our sample, which is a 100 nm thick silicon film, consisting of randomly oriented micro-crystallites (amorphous silicon a-Si). The transmitted beam was launched into a scanning grazing incidence monochromator the output of which was connected to a lock-in amplifier. The laser and gas jet parameters have been optimized to maximize the signal at around 100 eV, where we wanted to study dynamical structure modifications of silicon via changes of absorption near the L-edge. The signal has been safely above the noise level up to energies of about 500 eV opened the way to EXAFS (Rehr 2000). A small fraction of the output beam energy was delayed and focused onto the sample obtaining a pump fluence nearly two orders of magnitude below the damage threshold. Due to chopping of the pump beam and using a lock in amplifier it was now easily possible to detect changes of the transmitted spectra as small as a 10^{-4} .

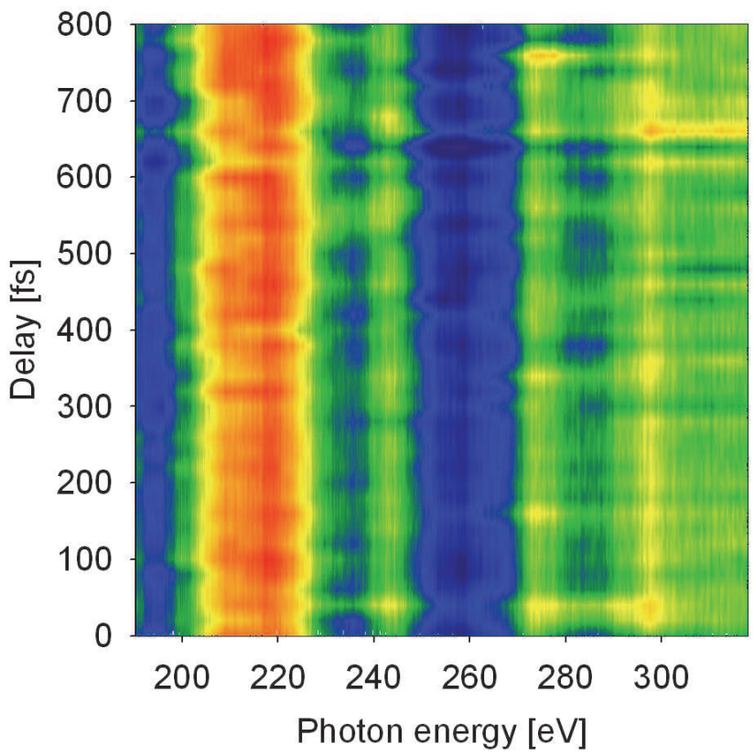

Fig. 7. Measured x-ray absorption difference spectra above the silicon L- edge after excitation with an ultrashort laser pulse. The delay has been varied in 20 fs steps in a range up to to 800 fs. From these data we can calculate via EXAFS the evolution of the interatomic distances.

To follow structural changes we opted for EXAFS (Oguri 2005, Brown 1999). From the measured absorption curves, the EXAFS signals $\chi(k)$ were calculated as a function of photoelectron wave number (k given in $Å^{-1}$) and from the measured absorption coefficient, the slowly varying contribution of the single atom absorption have been

eliminated with a high pass filter. After applying an amplitude window function and weighting the data with k^2, the atomic distance has been evaluated from the power density spectrum. The estimated interatomic distances are 2.20 ± 0.02 Å for Si which agrees very well with measurements at synchrotrons (Glover 2003). These measurements clearly demonstrate that it is possible generate HH signal up to several keV and the photon flux is sufficient for x-ray absorption spectroscopy. These results are the basis for our subsequent experiments, which made it possible to follow atomic motions in disorder materials with time resolved EXAFS.

The x-ray absorption spectra have been recorded in delay range of -300 fs to 800 fs in steps of 20 fs. The evaluation of the EXAFS signal gives the averaged atomic distances at the instant of probing. The calculated atomic distance shows a fast and slow oscillatory motion as a function of the delay. We fitted to the data the sum of two sinusoidal waves and found the best agreement for frequencies of 3.1 THz and 17 THz, respectively (Seres E 2007, Seres E 2008). As a check of the reliability of our evaluation and to minimize the influence of amplitude and phase noise we calculated the two dimensional FT of the whole data set. The evaluated spectrum shows again two distinct maxima at 3.6 THz and 17 THz. With two independent evaluation methods namely two-dimensional FT and least square fitting we identified two dominating oscillations at the same frequencies, making us confident that we have observed atomic oscillations. Moreover these frequencies agree very well with the predicted numbers for coherent phonons in Si after laser pulse excitation and have been published recently (Seres 2006, 2008, 2009).

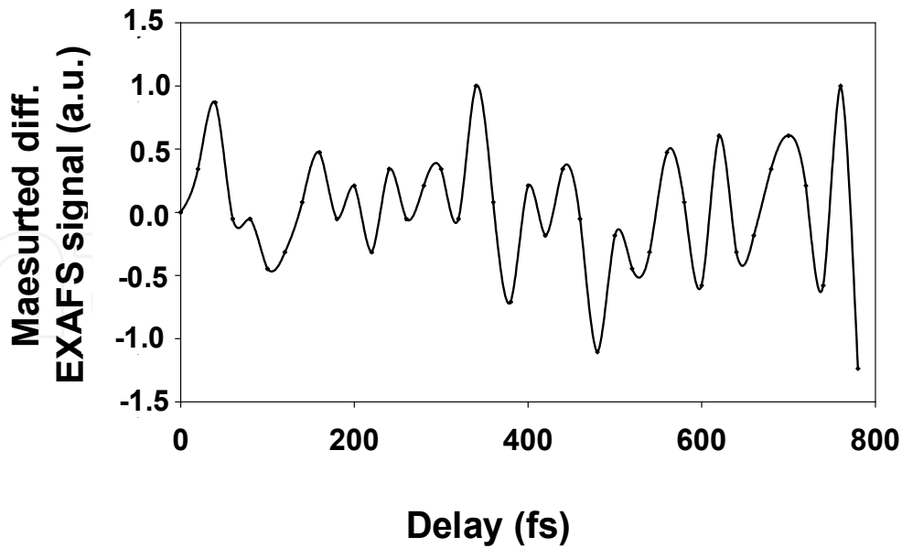

Fig. 8. The evaluated time resolved EXAFS signal at the Si L edge.

5.2 Changes in the atomic electronic levels, orbits

Most electronic devices have yet a limited temporal resolution, which prevent to detect fast electronic, magnetic changes on the atomic or molecular scale. But these changes come always together with the changing of the optical parameters in the x-ray regime. The absorption, reflection, or even the polarization of the x-ray light are sensitive to the electronic or magnetic states. Exciting a core electron from the valence level into the conduction level, the absorption cross-section is influenced by the changed density-of state (DOS) (Figure 9).

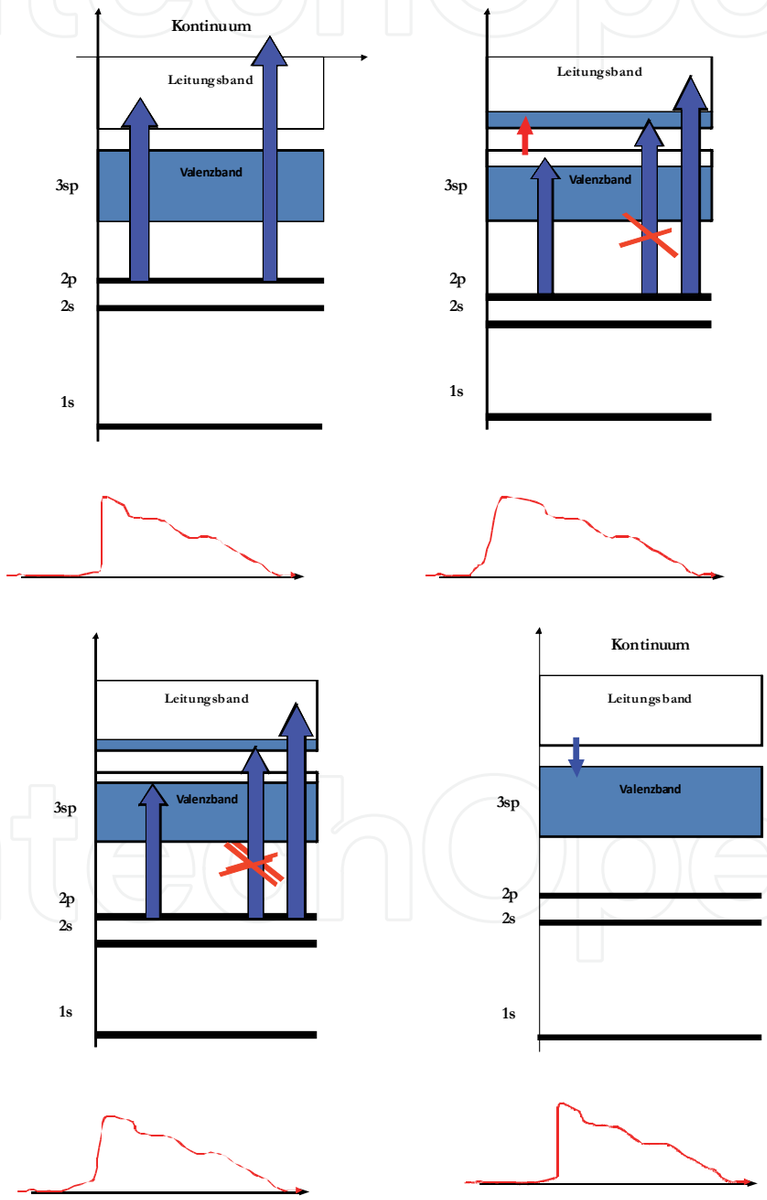

Fig. 9. The form of the absorption edge follows the changes of the electronic states produced by excitation.

A similar setup as for the time resolved EXAFS can record not only the atomic motion but the electronic changes after the short pump laser pulse. The laser pump light is absorbed through single and two photon absorption, creating a non-thermal electron distribution in the conduction band. The hot electron distribution thermalizes over different channels and time scales such as fast inter band thermalization via electron–phonon scattering and finally on a longer time-scale via recombination. The excitation of the electrons creates occupied states in the conduction band and unoccupied states in the valence band. These modifications have their signature also in the fine-structure of the soft-x-ray absorption spectrum (Nakano 1999).

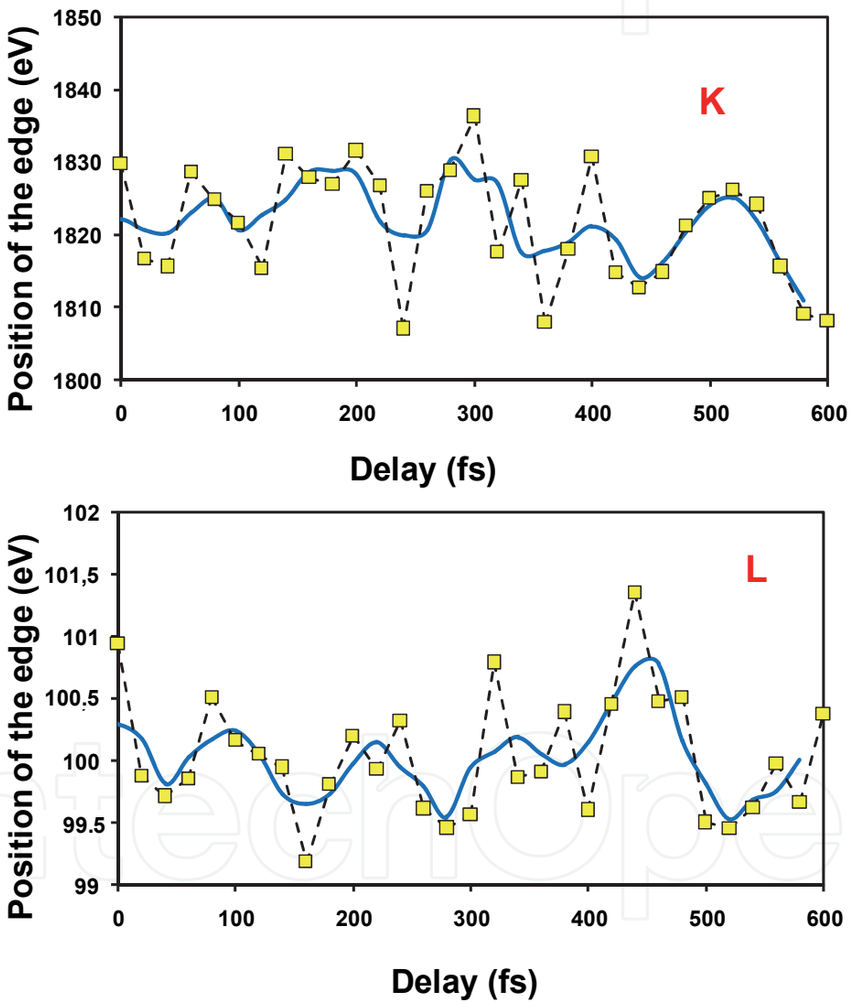

Fig. 10. Measured shift of the position of the (a) K- edge (1.8k eV) and (b) L-edge (100 eV) of silicon after excitation with an ultrahsort laser pulse (Seres 2009).

To investigate the carrier dynamic we recorded the difference absorption spectra in the vicinity of the L and K-edge of silicon as a function of the delay. The measured difference spectrum has been modified in very complex way and a full analysis would require a detailed knowledge about the exact band structure. To gain some information about the

relevant time constants we calculated the expectation value of the difference signal near the edge. The position of the L and K absorption edge of silicon oscillate with different amplitude and frequency as shown in Fig. 10. From a long-range measurement we have identified a fast and a slow time constant. The fast time constant is in the order of approx. 200 fs and the slow one in the order of 50 ps (Seres 2005). Comparing our findings with experiments based on conventional optical spectroscopy of silicon the fast time constant of about 200 fs is in reasonable agreement with the previously observed electron-phonon relaxation time in a-Si. The longer time constant of about 80ps corresponds to the carrier recombination time of electron and holes across the Si band gap (Sundram 2002).
Our pulsed XUV source delivering sub-20 fs pulses in an energy range up to 3 keV is bright enough for time-resolved XANES experiments. In a series of proof-of-principle experiments we have studied the electronic dynamics of the amorphous silicon bove the Si L edge and the C K edge, respectively. Further measurements are necessary to explore the underlying physics in full detail.

6. Acknowledgements

Financial support from the Deutsche Forschungsgemeinschaft (grant SE 1911/1-1 and TR 18, P10), the State of Thuringia (grant TMBWK B 715-08008) and the Friedrich Schiller University (grant ProChance 2009 A1) is gratefully acknowledged. We would like to express special thanks to all colleagues who have contributed to this work by supporting us with discussions and material.

7. References

Agarwal, B. K. (1991). *X-Ray Spectroscopy* Springer Verlag, Berlin

Ammosov, M. et al. (1986). Tunnel ionization of complex atoms and of atomic ions in an alternating electromagnetic field. *Sov. Phys. JETP* Vol. 64, pp. 1191-1194

Antoine, P. et al., (1996). Generation of attosecond pulses in macroscopic media. *Phys. Rev. A*, Vol. 56, No. 6 (December 1996), pp. 4960-4969

Bianconi, A et al., (1987). Multiple-scattering effects in the K-edge x-ray-absorption near-edge structure of crystalline and amorphous silicon. *Phys. Rev. B.* Vol. 36, No. 12, (October 1987) pp. 6426-6433

Brabec T. and Krausz, F. (2000). Intense few-cycle laser fields: Frontiers of nonlinear optics. *Rev. Mod. Phys.* Vol. 72, No. 2, (April 200), pp. 545-591

Bressler, Ch. et al., (2002). Towards structural dynamics in condensed chemical systems exploiting. *J. Chem. Phys.*, Vol. 116, No. 7, (February 2002), pp. 2295-2966

Bressler, Ch., Chergui M. (2004). Ultrafast X-ray Spectroscopy *Chem. Rev.*, Vol. 104, No. 4, pp. 1781-1812

Brown, F. L. H., et al. (1999). Ultrafast extended x-ray absorption fine structure (EXAFS)-theoretical considerations *J. Chem. Phys.*, Vol. 111, No. 14, (October 1999), pp. 6238-6246

Bzowski, S. A., & Sham T. K. (1993). Pd-Ti bimetallic: A study of the electronic structure using X–ray photoelectron spectroscopy and x-ray-absorption near-edge structure *Phys. Rev. B.* Vol. 48, No.11, (September 1993), pp. 7836-7840

Christov, I. P. et al., (1997). High-Harmonic Generation of Attosecond Pulses in the "Single-Cycle" Regime. *Phys. Rev. Lett.* 78, No. 7, (February 1997), pp. 1251-1254

Constant e., et al., (1999). Optimizing High Harmonic Generation in Absorbing Gases: Model and Experiment. *Phys. Rev. Lett.* Vol. 82, No. 8, (February 1999), pp. 1668-1671

D'Angelo, P. et al., (1996). Multi electron excitations at the L edges of barium in aqueous solution. *Phys. Rev. B.* Vol. 54, No. 17, (November 1996), pp. 12129-12138

Da Silva, L. B. et al., (1994). Generation of a 45-ps-duration 15.5-nm x-ray laser. *Opt. Lett.* Vol 19, No. 19, pp. 1532-1534

Ditmire, T. et al., (1995). Energy-yield and conversion-efficiency measurements of high-order harmonic radiation. *Phys. Rev. A*, Vol. 51, No. 2, (February 1995), pp. R902-R905

Faraci, G., et al., (1997). XANES of high-pressure Kr clusters in Be and Si. *Phys. Rev. B.,* Vol. 56, No. 19, (November 1995), pp. 12553-12559

Farges, F., et al.,(1997). Ti K-edge Xanes studies of Ti coordination and disorder in oxide compounds: Comparison between theory and experiment. *Phys. Rev. B.* Vol. 56, No. 4, (July 1997), pp. 1809-1819

Filiponi, A., et al., (1989). Structural investigations of a-Si and a-Si:H using X-ray-absorption spectroscopy at the Si K edge. *Phys. Rev. B.* Vol. 40, No. 14, (November 1989), pp.9636-9643

Gibson, E. A., et al. (2003). Coherent Soft X-ray Generation in the Water Window with Quasi–Phase Matching *Science,* Vol.302. No.3. (October 2003),8may 1995), pp. 95-98

Giulietti, D., & Gizzi, L. A. (1998). X-Ray Emission from Laser Produced Plasmas. *La Rivista del Nuovo Cimento*, Vol. 21, No.1, pp.1-103

Glover, C. J., Foran, G. J. & Ridgway, M.C. (2003). Structure of amorphous silicon investigated by EXAFS. Nucl. *Instr. And Meth. In Phys. Res. B*, Vol. 199, pp. 195-199

Gordon C. L. et al., (1995). Time-gated imaging with an ultrashort-pulse, laser-produced-plasma x-ray source*, Opt. Lett.,* Vol. *20*, No. 9, (Mai 1995), pp. 1056-1058

Johnson, S. L. et al. (2003). Properties of Liquid Silicon Observed by Time-Resolved X-Ray Absorption Spectroscopy. *Phys. Rev. Lett.,* Vol. 91, No. 15, (October 2003), pp. 157403

Kan, C. et al., (1997). Coherent XUV Generation from Gases Ionized by Several Cycle Optical Pulses. *Phys. Rev. Lett*. Vol. 79, No. 16, (October 1997), pp. 2971-2974

Kondo K. et al., (1993). Wavelength dependence of nonsequential double ionization in He. *Phys. Rev. A*, Vol. 48, No. 4, (October 1993), pp. R2531-R2533

Korobkin D., (1998). Soft X-Ray Amplification at 26.2 nm with 1-Hz Repetition Rate in a Table-Top System. *Phys. Rev. Lett*. Vol. 81, No. 8, (August 1998), pp. 1607-1610

Krainov, V. P. (1997).Ionization rates and energy-angular distributions at the barrier-suppression ionization of complex atoms and atomic ions *JOSA B* Vol. 14, No. 2, pp. 425-431

L'Huillier, A. & Balcou Ph. (1993). High-order harmonic generation in rare gases with a 1-ps 1053-nm laser. *Phys. Rev. Lett*. Vol. 70, No. 6, (February 1993), pp. 774-777

La-O-Vorakiat, C., et al., (2009). Ultrafast Demagnetization Dynamics at the M Edges of Magnetic Elements Observed Using a Tabletop High-Harmonic Soft X-Ray Source. *Phys. Rev. Lett.* Vol. 103, No. 25, (December 2009), pp. 257402

Lee, P. A. et al., (1981). Extended x-ray absorption fine structure – its strength and limitations as a structural tool. *Rev. Mod. Phys*. Vol.53, No. 4, (October 1981), pp. 769-806

Lemoff B. E. et al., (1995). Demonstration of a 10-Hz Femtosecond-Pulse-Driven XUV Laser at 41.8 nm in Xe IX. *Phys. Rev. Lett.* Vol. 74, No. 9, (February 1995) pp. 1574-1577

Lewenstein, M. ,et al. (1994). Theory of high-harmonic generation by low-frequency laser fields *Phys. Rev. A,* Vol. 49, No.3, (March 1994), pp. 2117-2132

Lytle, F. et al.,(1975). Theory of the extended x-ray-absorption fine structure II. Experimental Results and selected results. *Phys. Rev. B.* Vol. 11, No. 12, (March 1975), pp. 4825-4835

Macklin et al., (1993). High-order harmonic generation using intense femtosecond pulses. *Phys. Rev. Lett. Vol*. 70, No. 6, (February 1993), pp. 766-769

Michette A. and S. Pfautsch 1996, X-rays, the first hundred years, Wiley & Sons.

Murnane, M. M., et. al., (1991). Ultrafast X-ray Pulses from Laser-Produced Plasmas. *Science* Vol. 251,No. 4993, pp. 531-536.

Nagata Y. K., et al., (1993). Soft-x-ray amplification of the Lyman-α transition by optical-field-induced ionization. *Phys. Rev. Lett*. Vol. 71, No. 23, (December 1993), pp. 3774-3777

Nakano, H., et al., (1999). Time-resolved soft x-ray absorption spectroscopy of silicon using femtosecond laser plasma x rays. Appl. Phys. Lett. Vol. 75, No. 16, (October 1999), pp. 2350-2352

Nickles, P. V. et al., (1997). Short Pulse X-Ray Laser at 32.6 nm Based on Transient Gain in Ne-like Titanium. *Phys. Rev. Lett.* Vol. 78, No. 14, (April 1997) pp. 2748-2751

Oguri, K. et al.(2005). Transient observation of extended x-ray absorption fine structure in laser melted Si by using femtosecond laser-produced-plasma soft x ray. *Appl. Phys. Lett.* Vol. 87, (July 2005), pp. 011503

Paul, A. et al., (2003). Quasi-phase-matched generation of coherent extreme-ultraviolet light. *Nature* Vol. 421, (January 2003), pp. 51-54

Perry, M. D., & Crane J. K. (1993). High-order harmonic emission from mixed fields. *Phys. Rev. A*, Vol. 48, No. 6 (December 1993), pp. R4051-R4057

Raksi, F., et al.,(1996). Ultrafast x-ray absorption probing of a chemical reaction. *J. Chem. Phys.* Vol. 104, No. 15, (April 1996), pp. 6066-6069

Rehr J. J. & Albers R. C. (2000). Theoretical approaches to x-ray absorption fine structure. *Rev. Mod. Phys.* Vol. 72, No. 3, (July 2000), pp. 545-591

Rehr J. J. et al., (1992) High-Order-Multiple-Scattering Calculations of X-Ray-Absorption Fine Structure *Phys. Rev.Lett.*, Vol. 69, No. 23, (December 2002), pp. 3397-3400

Rischel, C., A., et al., (1997). Femtosecond time-resolved X-ray diffraction from laser-heated organic films . *Nature*, Vol. 390, (September 1997), pp. 490-492

Rocca, J. J. et al., (1994). Demonstration of a Discharge Pumped Table-Top Soft-X-Ray Laser, *Phys. Rev. Lett.* Vol. 73, No. 16, (October 1994), pp. 2192-2195

Rose-Petruck, C., et al., (1999). Picosecond-milliangstroem lattice dynamics measured by ultrafastX-ray diffraction. *Nature* Vol. 398,(25 March 1999), pp. 310-312

Rousse, A., et al. (2001). Femtosecond x-ray crystallography. *Rev. Mod. Phys.* Vol. 7317, No.1 pp. 17-31

Salieres, S. et al., (1995). Coherence Control of High-Order Harmonics. *Phys. Rev. Lett.* Vol. 74, No. 19, (Mai 1995), pp. 3776-3779

Salieres, S. et al., (1999). Study of the spatial and temporal coherence of high-order harmonics. *Adv. Atom. Mol. Opt. Phys.* Vol. 41, pp. 83-142

Schnürer, M. et al., (1999). Absorption-Limited Generation of Coherent Ultrashort Soft-X-Ray Pulses. *Phys. Rev. Lett.* Vol. 83, No. 4 (July 1999), pp. 722- 725

Schnürer, M., et al., (1998). Coherent 0.5keV x-ray emission from helium driven by a sub-10 fs laser. *Phys. Rev. Lett.* Vol. 80, No. 15, (April 1998) 3236.

Scrinzi, A., et al. (1999). Ionization above the Coulomb Barrier. *Phys. Rev. Lett.* Vol. 83, No.4, (July 1999), pp. 706-709

Seibert, M. M. et al., (2010). Femtosecond diffractive imaging of biological cells. *J. Phys. B,* Vol. 43, (September 2010), pp. 194015

Seres E. (2005) PhD Thesis, University of Würzburg

Seres, E., & Spielmann, C. (2007). Ultrafast soft x-ray absorption spectroscopy with sub-20-fs resolution. *Appl. Phys. Lett.* Vol. 91, No. 12, (September 2007), pp. 121919

Seres, E. et al. (2006). X-ray absorption spectroscopy in the keV range with laser generated high harmonic radiation. *Appl. Phys. Lett.* Vol. 89, (November 2006), pp. 181919

Seres, E. et al., (2003). Sub-10-fs, terawatt-scale Ti:sapphire laser system. *Opt. Lett*. Vol. 28, No. 19. (October 2003). Pp. 1832-1834

Seres, E. et al., (2004). Generation of Coherent Soft-X-Ray Radiation Extending Far Beyond the Titanium L Edge. Phys. Rev. Lett. Vol. 92, No. 16, (April 2004), pp. 163002

Seres, E. Seres, J. & Spielmann, Ch. (2009). Time resolved spectroscopy with femtosecond soft-x-ray pulses. Appl. Phys. A, Vol. 95, pp. 43-50

Seres, E., & Spielmann, Ch. (2008). Time-resolved optical pump X-ray absorption probe spectroscopy in the range up to 1 keV with 20 fs resolution. *J. Mod. Opt.* Vol. 55, No. 16, (September 2008), pp. 2643–2651

Seres, J. et al. (2006a). Generation of coherent keV x-rays with intense femtosecond laser pulses. *New. J. Phys.* Vol. 8 , (October 2006), pp. 251

Seres, J., et al. (2005). Source of coherent kiloelectronvolt X-rays. *Nature,* Vol., 433, (February 2005), pp. 596

Seres, J., et al.(2007). Coherent superposition of laser-driven soft-X-ray harmonics from successive sources. *Nature Phys.* Vol.3, (December 2007), pp. 878-883

Sipr, O., (2002). Spatial Distribution of photoelectrons participating in formation x-ray absorption spectra *Phys. Rev. B*. Vol. 65, No. 20, (Mai 2002), pp. 205115

Sommerer, G. rottke H., & Sandner W. (1999). Enhanced Efficiency in High-Order Harmonic Generation Using Sub-50-fs Laser Pulses. *Laser Phys.* Vol. 9, No. 1, pp. 430-432

Spielmann, Ch. et al, (1998). Ultrafast near-keV coherent x-ray sources pumped by sub-10fs lasers, IEEE JSTQE 4, 249

Spielmann, Chet al.,(1997). Generation of coherent x-ray in the water window using 5-fs laser pulses. *Science*, 278, 661.

Stern, E. A., (1974). Theory of the extended x-ray-absorption fine structure. *Phys. Rev. B.*Vol. 10, No. 8,(October 1974),pp. 3027-3037 (1974)

Sundaram, S. K. & Mazur, E. (2002). Inducing and probing non-thermal transitions in semiconductors using femtosecond laser pulses. *Nature Mater. Vol.* 1, (December 2002),pp. 217-224

Tempea, G., et al. (2000). Self-Phase-Matched High Harmonic Generation. *Phys. Rev. Lett.*, Vol.84, No. 19,(Mai 2000), pp. 4329-4332

Umstadter et al., (1998). Tabletop, Ultrahigh-Intensity Lasers: Dawn of Nonlinear Relativistic Optics.Opt. &Photon. News Vol. 9. Iss. 7.pp. 40-

Wahlstroem, C.-G., (1993). High-order harmonic generation in rare gases with an intense short-pulse laser. *Phys. Rev. A*, Vol. 48, No. 6, (December 1993), pp. 4709-4720

Walser, M. M., et al., (2000). High Harmonic Generation Beyond the Electric Dipole Approximation. *Phys. Rev. Lett.*, Vol. 85, No. 24, (December 2000), pp. 5082-5085

Woerner, H. J., et al. (2010). High-Harmonic Homodyne Detection of the Ultrafast Dissociation of Br_2 Molecules. *Phys. Rev. Lett.* Vol. 105, (September 2010), pp. 103002

Zepf, M. et al., (2007). Bright Quasi-Phase-Matched Soft-X-Ray Harmonic Radiation from Argon Ions. *Phys. Rev. Lett.* Vol. 999, (October 2007), pp. 143901

Zewail, A. H. (2000). Femtochemistry: Atomic-Scale Dynamics of the Chemical Bond. *J. of Phys. Chem.* A, Vol.104,(Mai 2000), pp. 5660-5694

Zhang, J. et al., (1997). A Saturated X-ray Laser Beam at 7 Nanometers. *Science* vol. 276, no. 5315, (Mai 1997) pp. 1097-1100

Zhou J. et al., (1996). Enhanced High-Harmonic Generation Using 25 fs Laser Pulses. *Phys. Rev. Lett.* Vol. 76, No.5, (January 1996), pp. 752-755

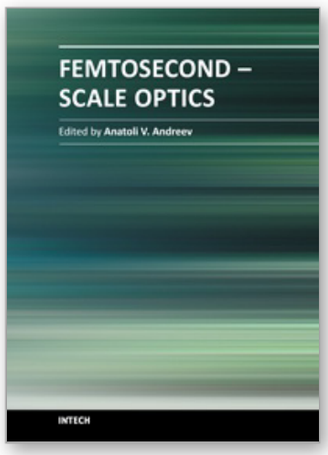

Femtosecond-Scale Optics
Edited by Prof. Anatoly Andreev

ISBN 978-953-307-769-7
Hard cover, 434 pages
Publisher InTech
Published online 14, November, 2011
Published in print edition November, 2011

With progress in ultrashort ultraintense laser technologies the peak power of a laser pulse increases year by year. These new instruments accessible to a large community of researchers revolutionized experiments in nonlinear optics because when laser pulse intensity exceeds or even approaches intra-atomic field strength the new physical picture of light-matter interaction appears. Laser radiation is efficiently transformed into fluxes of charged or neutral particles and the very wide band of electromagnetic emission (from THz up to x-rays) is observed. The traditional phenomena of nonlinear optics as harmonic generation, self-focusing, ionization, etc, demonstrate the drastically different dependency on the laser pulse intensity in contrast the well known rules. This field of researches is in rapid progress now. The presented papers provide a description of recent developments and original results obtained by authors in some specific areas of this very wide scientific field. We hope that the Volume will be of interest for those specialized in the subject of laser-matter interactions.

InTech Europe
University Campus STeP Ri
Slavka Krautzeka 83/A
51000 Rijeka, Croatia
Phone: +385 (51) 770 447
Fax: +385 (51) 686 166
www.intechopen.com

InTech China
Unit 405, Office Block, Hotel Equatorial Shanghai
No.65, Yan An Road (West), Shanghai, 200040, China
中国上海市延安西路65号上海国际贵都大饭店办公楼405单元
Phone: +86-21-62489820
Fax: +86-21-62489821

IntechOpen